Two Dimensional Imaging Measurement of Magnetic Reconnection Outflow in the TS-4 Toroidal Plasma Merging Experiment*)

Hiroshi TANABE[a)], Hirotaka OKA, Masanobu ANNOURA, Akihiro KUWAHATA, Kazutake KADOWAKI, Yasuhiro KAMINOU, Setthivoine YOU[1)], Alexander BALANDIN[2)], Michiaki INOMOTO and Yasushi ONO

Graduate School of Frontier Sciences, The University of Tokyo, Tokyo 113-0032, Japan
[1)]*University of Washington, Seatle, Washington 98195-2250, USA*
[2)]*Institute of System Dynamics and Control Theory, Irkutsk 664033, Russia*

(Received 7 December 2012 / Accepted 10 April 2013)

A novel 2D toroidal plasma flow velocimetry has been developed using tomographic reconstruction technique. The 2D imaging of local (*R*-*Z*) toroidal velocity is achieved by the vector tomographic reconstruction technique and multi-chord 2D spectroscopy by 35-channel optical fiber array. Numerical simulation for reconstruction of bi-directional toroidal velocity profile suggests that the cost-effective arrangement of the optical fiber for a toroidal plane is 7. We installed the system with 7×5 chords arrangement to the TS-4 device. This system successfully measured 2D bi-directional toroidal velocity profile around X point with 10% accuracy during the counter-helicity magnetic reconnection experiment.

Keywords: Doppler shift, vector tomography, toroidal flow, magnetic reconnection, sling-shot

DOI: 10.1585/pfr.8.2405088

1. Introduction

The Doppler frequency shift is a popular remote sensing principle for various velocimetry. As a plasma diagnostics tool, the wavelength shift of the line-spectrum emission is widely used for measurement of plasma bulk flow. Unlike active spectroscopic techniques, such as LIF [1] or CXRS [2], in passive Doppler spectroscopy, the measured spectral line signal is integrated over each line-of-sight. Furthermore, the target plasma for LIF must be relatively dense or slow and it is often unsuitable when microsecond time resolution is required such as laboratory fusion and astrophysical experiment. Then, recent laboratory experiment often neglects the plasma perturbation of direct in-situ measurements, such as the ion dynamics spectroscopy (IDS) probe [3] inside the plasma but they should be used carefully for low temperature plasmas. To solve these problems of line-integrated effect for passive remote sensing, computer tomography has been widely used, initially for medical imaging of human body and recently for the measurement of physical parameter. In plasma diagnostics, remarkable success for ECE tomography of sawtooth crash in tokamaks [4] and 3D imaging of kink instability for magnetoplasmadynamic has been reported [5].

However, for the application of tomographic reconstruction of plasma flow, the object of the reconstruction is not scalar but vector quantity. Then radon transform of the local profile is changed from $\int_L V dl$ to $\int_L \boldsymbol{V} \cdot \boldsymbol{dl}$ (Fig. 1: vector radon transform), proper inversion technique is required [6]. In addition, plasma flow diagnostics by passive Doppler spectroscopy mostly uses Czerny-Turner Grating spectrometer having a slit which limits the spatial resolution to 1D. As a solution to these problems, this paper describes the novel 2D measurement of toroidal flow using vector tomography technique and 2D multi-chord spectroscopy system that was installed to TS-4 toroidal plasma. Section2 summarize the vector tomography technique for toroidal flow measurement. Section 3 describes a numerical simulation of the reconstruction method and Section 4 demonstrates this 2D diagnostic for the "toroidal sling shot" [7] during the magnetic reconnection experiment in TS-4.

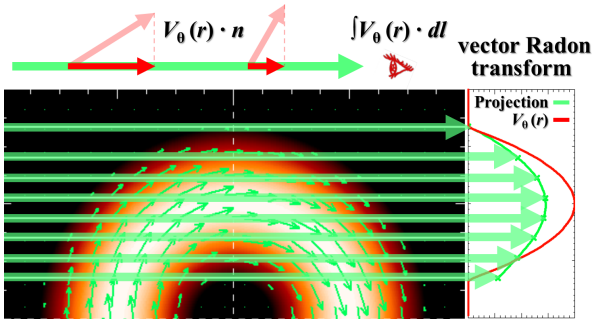

Fig. 1 The concept of the vector radon transform. Only the line-of-sight component of the vector field contributes to the projected velocity profile.

author's e-mail: tanabe@ts.t.u-tokyo.ac.jp
[a)] Research Fellow of the Japan Society for the Promotion of Science
*) This article is based on the presentation at the 22nd International Toki Conference (ITC22).

2. Inversion Method

2.1 Description of toroidal flow velocity by potential function

To solve the vector tomography problem, it is convenient to describe a vector field by potential function. Generally, arbitrary vector field $\boldsymbol{V}(x, y)$ can be decomposed as follows by the Helmholtz decomposition theorem.

$$\boldsymbol{V} = \mathrm{grad}\Phi + \mathrm{rot}\boldsymbol{\Psi}, \tag{1}$$

where Φ and $\boldsymbol{\Psi}$ are the scalar and vector potential functions, while $\mathrm{grad}\Phi$ and $\mathrm{rot}\boldsymbol{\Psi}$ are the solenoidal and irrotational parts of $\boldsymbol{V}$, respectively. For line-integrated Doppler spectroscopy measurement, the first term contributes as spectral broadening and the second term does as the bulk Doppler shift. In axisymmetric torus plasma, toroidal flow velocity V_θ can be described by the Z component of the vector potential $\boldsymbol{\Psi} = \psi \boldsymbol{e}_z$ [8]. Then, for the toroidal flow measurement geometry, the vector field reconstruction problem is converted (simplified) to a scalar tomography problem to reconstruct the potential function ψ.

The reconstruction of the Z component of the vector potential ψ uses the constraints $\nabla^2\psi = -\omega$ with vorticity $\omega = rot\boldsymbol{V}$.

$$\frac{\partial}{\partial y}\int_L \boldsymbol{V}\cdot\boldsymbol{dl} = \int_L \omega dl = -\int_L \nabla^2\psi dl, \tag{2}$$

$$f(y) = \int_L \boldsymbol{V}\cdot\boldsymbol{dl} = -\frac{\partial}{\partial y}\int_L \psi dl, \tag{3}$$

$$\int f(y)dy = \int\Big(\int_L \boldsymbol{V}\cdot\boldsymbol{dl}\Big)dy = -\int_L \psi dl. \tag{4}$$

Then, using the Abel inversion to $\int_L \psi dl$,

$$\begin{aligned}\psi(r) &= -\frac{1}{\pi}\int_r^R \frac{\partial}{\partial y}\Big(-\int f(y)dy\Big)\frac{1}{\sqrt{y^2-r^2}}dy \\ &= \frac{1}{\pi}\int_r^R \frac{f(y)}{\sqrt{y^2-r^2}}dy = \frac{1}{\pi}\int_r^R \frac{\int_L \boldsymbol{V}\cdot\boldsymbol{dl}}{\sqrt{y^2-r^2}}dy.\end{aligned} \tag{5}$$

Finally, taking the curl of the potential ψ, toroidal rotation profile is described as follows.

$$\boldsymbol{V}_\theta(x, y) = \Big(\frac{\partial\psi(x, y)}{\partial y}, -\frac{\partial\psi(x, y)}{\partial x}\Big), \tag{6}$$

$$\text{or}\quad V_\theta(r) = \frac{\partial\psi(r)}{\partial r}. \tag{7}$$

2.2 Spectral moment analysis for "line-integrated" Doppler shift evaluation

In the Doppler spectroscopy measurement, the vector tomography analysis needs proper data input format. The spectral peak shift obtained by the Gaussian fitting is precisely not $\int_L \boldsymbol{V}\cdot\boldsymbol{dl}$ and the local line spectra are integrated through the sight line of the detector as following.

$$f(y, \lambda) = \int_L I_0(r)\exp\Big[-\frac{1}{2}\Big(\frac{\lambda-\lambda_0-\Delta\lambda_D(r)}{\sigma_D(r)}\Big)^2\Big]dl, \tag{8}$$

$$I_0(r) = \frac{\epsilon_0(r)}{\sqrt{2\pi}\sigma_D(r)}, \Delta\lambda_D(r) = \frac{\lambda_0}{c}\boldsymbol{V}(r)\cdot\boldsymbol{n}. \tag{9}$$

Here, $\boldsymbol{n}$ is a normalized line-of-sight vector and σ_D is line broadening ($FWHM = 2\sigma_D(r)\sqrt{2ln2}$). The spectral peak shift of the line-integrated spectra $f(r, \lambda)$ is line-averaged Doppler shift with the weight of emission and is not the proper input parameter for the tomographic reconstruction.

For a proper inversion, we introduce spectral moment

$$\mu^n(r) = \int_{-\infty}^{\infty} f(r, \lambda)\lambda^n d\lambda, \tag{10}$$

$$\mu^0(r) = \int_{-\infty}^{\infty} f(r, \lambda)d\lambda = \int_L \epsilon_0(r)dl, \tag{11}$$

$$\mu^1(r) = \int_{-\infty}^{\infty} f(r, \lambda)\lambda d\lambda = \int_L \epsilon_0(r)\Delta\lambda_D(r)dl \tag{12}$$

$$\propto \int_L \epsilon_0(r)\boldsymbol{V}(r)\cdot\boldsymbol{n}dl.$$

The zeroth moment is the line-integrated emission and the first moment is the line-integrated Doppler shift with the weight of emission. Then, $\epsilon_0(r)\boldsymbol{V}(r)$ is obtained by applying the vector tomography reconstruction for $\mu^1(y)$: the first moment of the measured spectra in each viewing chord. In spectroscopy measurement, $f(y)$ is $\mu^1(y)$, then radial vector potential profile $\psi(r)$ to describe $\epsilon_0(r)\boldsymbol{V}(r)$ is obtained by substituting $\mu^1(y)$ for $f(y)$ in eq. (5)

$$\psi(r) = \frac{1}{\pi}\int_r^R \frac{\mu^1(y)}{\sqrt{y^2-r^2}}dy. \tag{13}$$

The weight $\epsilon_0(r)$ is also measured by using scalar tomography for the zeroth moment.

$$\epsilon_0(r) = -\frac{1}{\pi}\int_r^R \frac{\partial\mu^0(y)}{\partial y}\frac{1}{\sqrt{y^2-r^2}}dy. \tag{14}$$

Finally, the toroidal velocity profile $\boldsymbol{V}(r)$ is reconstructed as follows:

$$\boldsymbol{V}(x, y) = \frac{1}{\epsilon_0(r)}\Big(\frac{\partial\psi(x, y)}{\partial y}, -\frac{\partial\psi(x, y)}{\partial x}\Big), \tag{15}$$

$$\text{or}\quad V_\theta(r) = \frac{1}{\epsilon_0(r)}\frac{\partial\psi(r)}{\partial r}. \tag{16}$$

3. Estimation of the Number of Cost-Effective Viewing Chords

The verification of the reconstruction technique was numerically tested by Balandin in 2001 [6]. Here we evaluate the number of cost-effective viewing chords for the possible velocity profile in our TS-4 plasma merging experiment to construct 2D toroidal flow measurement.

- Model 1: toroidal sling-shot velocity profile [9]
- Model 2: parabolic toroidal velocity profile [10]

For the simulation, spectral resolution is set as 0.00118 nm/pixel, $T_i = 20$ eV, wavelength is 434.80635 nm (ArII) and the maximum velocity is set as 20 km/s. To set the test profile for the two velocity profiles, we use the

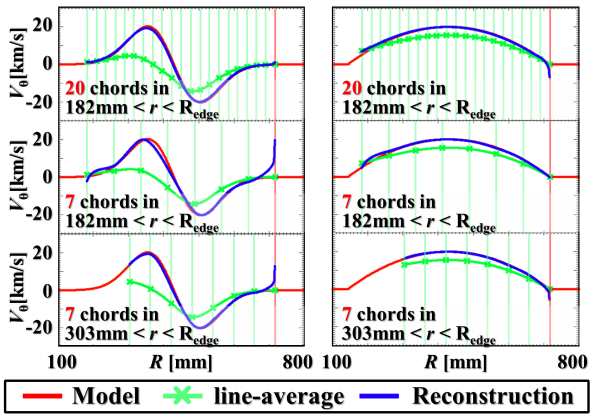

Fig. 2 The result of the numerical test of reconstruction for two types of toroidal flow velocity profile (red). Line-averaged profile (green) tends to be smoothed by the effect of line-integration. The number of viewing chords (or how dense it is) decides the reconstruction accuracy.

following mathematical model,

$$V_{\theta_1} = A\exp\Big(-\frac{1}{2}\frac{(r-r_{\mathrm{Xpoint}})^2}{\sigma^2}\Big)\Big(\frac{(r-r_{\mathrm{Xpoint}})}{\sigma^2}\Big), \quad (17)$$

$$A = -2.5\times10^6, \quad \sigma = 75, \quad r_{\mathrm{Xpoint}} = 430,$$

$$V_{\theta_2} = -a(r-r_{\mathrm{major}})^2 + V_{\mathrm{max}}, \quad (18)$$

$$a = 2.43\times10^{-1}, V_{\mathrm{max}} = 2.0\times10^4, r_{\mathrm{major}} = 430.$$

Then, line-integration of the spectral signal is performed by eq. (8) and the constraints of vector Radon transform is described using eq. (9).

Figure 2 is the result of the simulation for both two models with 20 or 7 chords measurement. The velocity profile of the model 1 and 2 are shown for "model" (test profile), "line-average" (measured by the Gaussian fitting of the chord-integrated spectra) and "reconstruction", respectively. For the discrete chord tomography measurement, the line-integrated Doppler shift (first moment) $\mu^1(y)$ is precisely $\mu^1(y_n)$ (n = 1,2,3...) and it is interpolated before using eq. (13). Then, the accuracy of the interpolation depends on the number of viewing chords and the structure of the target velocity profile. The numerical instability near the boundary ($r \sim R_{\mathrm{edge}}$) is caused by $\epsilon_0(r)$ which is ~ 0 near the edge in eq. (16). Therefore, reconstructed result must be adopt in the region $\epsilon_0(r) > 0$ by referring the result of eq. (14).

The difference between exact and reconstructed $V_\theta(r)$ is evaluated quantitatively by the following formula [8]:

$$\Delta^2 = \frac{\sum_{k=1}^{n}(V_{\theta\_k} - \overline{V}_{\theta\_k})^2}{\sum_{k=1}^{n}\overline{V}_{\theta\_k}^2}, \quad (19)$$

where $\overline{V}_{\theta\_k}$ and V_{θ_k} are the assumed and reconstructed toroidal velocity at the kth nodes of the grid and the summation covers all grid points in the following range which satisfies the constraint of $\epsilon_0(r) > 0$.

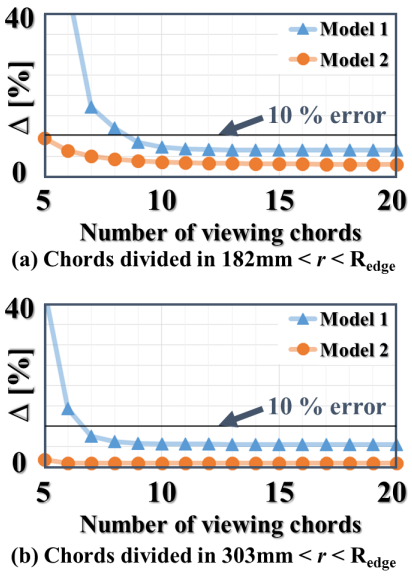

Fig. 3 Reconstruction error Δ as a function of the number of viewing chords. It depends on the complexity of the profile and the density of viewing chords in the target region, while tends to saturate even if adequate number of viewing chords are installed, indicating the existence of the cost-effective solution to upgrade the resolution to 2D.

(a) 182 mm $< r <$ 680 mm
(when chords divided in 182 mm $< r < R_{\mathrm{edge}}$)
(b) 303 mm $< r <$ 680 mm
(when chords divided in 303 mm $< r < R_{\mathrm{edge}}$)

Figure 3 plots Δ as a function of the number of viewing chords. The reconstruction error Δ is suppressed by increasing the spatial resolution of the line-integrated projection measurement, while tends to saturate once it goes less than 10%. This characteristics suggests the existence of cost-effective solution to upgrade the local diagnostics to 2D with limited chords spectroscopy measurement. For example, in our spectroscopy measurement application, the number of viewing chords is limited to 35 [11]. To apply it to a 2D measurement, possible 2D (R-Z) resolution is 7×5, 8×4 and so on. When the target measurement range is 182 mm $< r < R_{\mathrm{edge}}$, 8×4 system or more resolution for radial resolution is required to suppress $\Delta < 15\%$. While if 303 mm $< r < R_{\mathrm{edge}}$ is enough, 7×5 system can still work less than 10% error.

4. Experiment

4.1 2D Doppler tomography system

A 35 core optical fiber array (core width 230 μm) coupled with 7×5 ($R\times Z$) lenses collecting the 2D projection of plasma emission was used to make the 2D (R-Z) measurement of the toroidal flow velocity profile. In order to suppress the reconstruction error to less than 10% for the 7 chords toroidal measurement, the line-of-sight position is set as follows:

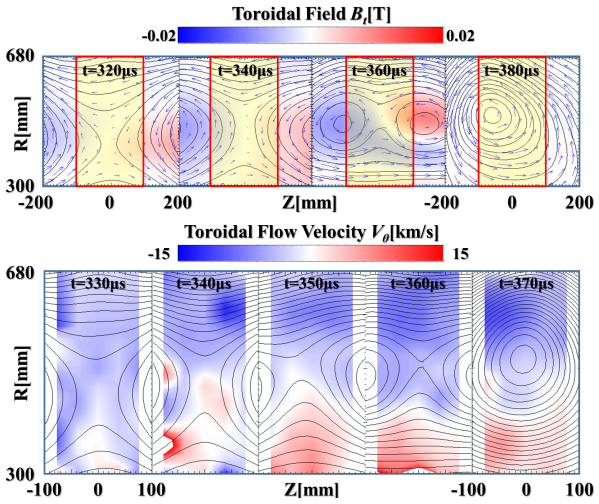

Fig. 4 The time evolution of the 2D toroidal flow velocity profile during the counter-helicity spheromak merging experiment in TS-4. The measurement position is indicated by the red rectangular box in the magnetic flux plot (top).

- $z = -76, -38, 0, 38, 76$ mm
- $r = 303.8, 362.8, 420.5, 476.5, 530.5, 582.5, 632.5$ mm (tangentially slices 5 toroidal plane)

This 2D projection composed of the 35 channels of line-spectrum emissions is transported through 35 optical fibers. They are realigned to 35×1 array for a 1.0 m polychromator connected with ICCD image sensors (1024×1024 pixel, 13 μm^2/pixel) through a magnifying optics (for the wavelength resolution of 0.00118 nm/pixel and for the correction of astigmatism). The vector tomographic reconstruction is performed for each 7 chords toroidal measurement at $z = -76, -38, 0, 38, 76$ mm, finally 2D toroidal flow velocity profile is obtained.

4.2 2D toroidal sling-shot measurement during counter helicity merging in TS-4

To demonstrate the 2D toroidal flow measurement, the vector tomography technique was applied for the counter-helicity spheromak merging experiment in TS-4. The toroidal sling-shot effect of magnetic reconnection generates a bi-directional toroidal flow structure around the X-point [10]. Alfven velocity for the experimental condition ($n_e \sim 1 \times 10^{20}$ m^{-3} and toroidal component of reconnecting field $B_t \sim 0.02$ T) is ~ 20 km/s for hydrogen plasma with 10% impurity argon. Figure 4 is the measured 2D toroidal flow velocity and magnetic field profile. With the time scale of 10-20 μs, localized toroidal acceleration develops as a 2D global structure and sub-Alfvenic acceleration is observed. The experimental error mostly comes from the grating smile calibration error caused by the small oscillation of the optics inside spectrometer with $\sim \pm 2$ pixel $\sim \pm 1.6$ km/s. The numerical instability near the peripheral region is removed by adopting the result only inside the core region 303.8 mm $< r <$ 680 mm.

5. Conclusion

A novel 2D toroidal flow imaging system has been developed by the application of 2D multi-chord spectroscopy to the vector tomography technique. The numerical simulation suggests the existence of cost-effective solution for a target velocity profile. For the measurement of toroidal acceleration in counter-helicity merging experiment in TS-4, reconstruction error can be suppressed to less than 10% to set 7 viewing chords in 303.8 mm $< r <$ 680 mm. Although the spatial resolution of this proposed method is less than the J. Howard's coherence imaging technique [12], it should be noted that the proposed 2D measurement allows to use a standard spectroscopy instrument, Czerny-Turner grating spectrometer with flexibility for wavelength and high spectral resolution, for 2D imaging application.

Acknowledgements

This work is supported by a Grant-in-Aid for Scientific Research (A) No. 22246119 and (B) No. 19340170, JSPS Core-to-Core Program No. 22001, and NIFS Collaboration Research Programs (NIFS06KOAH02 and NIFS08KUTR023).

[1] A. Okamoto, S. Yoshimura, S. Kado and T. Masayoshi, J. Plasma Fusion Res. **80**, 12 (2004).
[2] R.J. Fonck, D.S. Darrow and K.P. Jaehnig, Phys. Rev. Lett. **29**, 6 (1984).
[3] A. Kuritsyn, D. Craig, G. Fiksel, M. Miller, D. Cylinder and M. Yamada, Rev. Sci. Instrum. **77**, 10F112 (2006).
[4] Y. Nagayama, M. Yamada, W. Park, E. Frederickson, A. Janos, K. Mcguire and G. Taylor, Phys. Plasmas **3**, 1647 (1996).
[5] F. Bonomo, P. Franz, G. Spizzo, L. Marrelli, P. Martin, F. Pa-ganucci, P. Rossetti, M. Signori, M. Andrenucci and N. Pomaro, Phys. Plasmas **12**, 1 (2005).
[6] A.L. Balandin, T. Tawara and Y. Ono, Eur. Phys. J.D. **14**, 97 (2001).
[7] Y. Ono, M. Yamada, T. Akao, T. Tajima and R. Matsumoto, Phys. Rev. Lett. **76**, 18 (1996).
[8] A.L. Balandin, Y. Murata and Y. Ono, Eur. Phys. J.D. **27**, 125 (2003).
[9] N.J. Conway, P.G. Carolan, J. McCone, M.J. Walsh and M. Wisse, Rev. Sci. Instrum. **77**, 10F131 (2006).
[10] Y. Ono, T. Matsuyama, K. Umeda and E. Kawamori, Nucl. Fusion **43**, 649 (2003).
[11] H. Tanabe, S. You, A. Kuwahata, S. Ito, M. Inomoto and Y. Ono, IEEJ Trans. FM. **130**, 8 (2010).
[12] J. Howard, A. Diallo, M. Creese, B.D. Blackwell, S.L. Allen, R.M. Ellis, G.D. Porter, W. Meyer, M.E. Fenstermacher, N.H. Brooks, M.E. Van Zeeland and R.L. Boivin, Rev. Sci. Instrum. **81**, 10E528 (2010).